

Scaling of Two-Dimensional Semiconductor Nanoribbons for High-Performance Electronics

Hao-Yu Lan,^{1,2} Shao-Heng Yang,^{1,2} Yongjae Cho,^{1,2,6} Jun Cai,^{1,2} Zheng Sun,^{1,2} Chenyang Li,^{4,5} Lin-Yun Huang,⁵ Thomas Beechem,^{2,3} Yi Wan,⁴ Lain-Jong Li,⁴ Joerg Appenzeller,^{1,2} and Zhihong Chen^{1,2}

¹*Electrical and Computer Engineering, Purdue University, West Lafayette, Indiana, USA*

²*Birck Nanotechnology Center, Purdue University, West Lafayette, Indiana, USA*

³*Mechanical Engineering, Purdue University, West Lafayette, Indiana, USA*

⁴*Materials Science and Engineering, National University of Singapore, Singapore*

⁵*Nexstrom Pte. Ltd., Singapore, Singapore*

⁶*Department of Physics, Dankook University, Cheonan, Chungcheongnam-do, South Korea*

**To whom correspondence should be addressed.*

E-mail: zhchen@purdue.edu

Abstract

Monolayer transition metal dichalcogenide (TMD) field-effect transistors (FETs), with their atomically thin bodies, are promising candidates for future gate-all-around (GAA) nanoribbon architectures. While state-of-the-art Si GAA nanoribbon transistors feature channel widths in the tens of nanometers, most reported TMD-based FETs remain limited to micrometer-scale dimensions, limiting their relevance for ultra-scaled electronics. In this work, we investigate the channel width scaling in nanoribbon transistors based on monolayer MoS₂ grown on 2-inch wafers, achieving widths of approximately 30–40 nm. Remarkably, nanoribbon width scaling enhances the on-current by 30–40%, reaching up to 700 μ A/ μ m for the smallest-width devices, while also improving the subthreshold slope (SS) to as low as 70 mV/dec. This enhancement is attributed to a stronger electric field at the nanoribbon edges without significant degradation from edge-related scattering. To further demonstrate the scalability of the nanoribbon device, we evaluate the variability of extremely scaled monolayer MoS₂ nanoribbon transistor arrays featuring a contact pitch of 60 nm and an effective oxide thickness (EOT) of approximately 0.9 nm. Beyond MoS₂, we extend the nanoribbon structure to WS₂ n-type and WSe₂ p-type FETs,

demonstrating a viable path toward complementary monolayer TMD nanoribbon FETs for future ultra-scaled electronics.

Introduction

Over the past half-century, silicon (Si) MOSFET technology has experienced two distinct scaling phases: geometric (classical) scaling and equivalent (effective) scaling¹. Initially, geometric scaling, also known as Dennard scaling, focused on reducing critical transistor dimensions, such as gate length, channel thickness, and oxide thickness. However, as gate lengths approached tens of nanometers, short-channel effects (SCEs) began significantly compromising Si planar transistor performance. By around 2000, geometric scaling slowed down, leading to a shift towards equivalent scaling. This new phase leveraged structural and material innovations—including strained silicon, silicon-germanium channels², high- κ /metal-gate stacks (HKMG)³, and FinFET architectures⁴—to sustain continued performance gains. Specifically, HKMG enabled further equivalent oxide thickness (EOT) scaling without increasing leakage, while FinFET designs improved electrostatic control and increased transistor density. Currently, advances are progressing toward more complex structures such as nanosheet FETs (NS-FETs)^{5,6}, nanoribbon FETs (RibbonFETs)⁷, and complementary FETs (CFETs)⁸. Nevertheless, silicon-based technologies are approaching their fundamental physical scaling limits⁷, underscoring the urgent need to explore alternative channel materials to enable further transistor scaling.

To address the fundamental scaling limits of silicon, two-dimensional (2D) transition metal dichalcogenides (TMDs) have emerged as promising candidates. Their atomically thin bodies provide exceptional electrostatic gate control, essential for suppressing short-channel effects (SCEs) in ultra-scaled devices^{9–16}. This advantage is particularly evident in monolayer (1L) TMDs, which ideally have passivated surfaces, ensuring superior stability and performance at the nanoscale. Recent advancements in 2D field-effect transistors (FETs) have already demonstrated encouraging performance, achieving on-state currents (I_{ON}) of several hundred $\mu\text{A}/\mu\text{m}$ at drain voltages (V_D) around 1 V for channel lengths under 100 nm^{15,17–30}. Notably, quasi-ballistic transport observed in 10-nm transistors using exfoliated trilayer indium selenide (InSe) and wafer-grown trilayer MoS₂ underscores the intrinsic potential of 2D semiconductors for extremely scaled

electronics^{15,21}. Nevertheless, fully leveraging these materials requires a comprehensive understanding of scaling impacts across lateral (channel and contact lengths), vertical (channel and oxide thickness), and width (nanoribbon) dimensions.

Both channel length and contact length critically influence lateral scaling. To mitigate short-channel effects (SCEs), vertical dimensions, such as channel thickness and oxide thickness, must be scaled accordingly. Scaling vertical dimensions directly reduces the electrostatic screening length, thereby enabling further length scaling. Thus, transistor scaling limits must consider both lateral (length) and vertical (thickness) dimensions simultaneously^{31,32}. In addition to length and thickness scaling, width scaling has become increasingly significant, particularly in gate-all-around (GAA) nanosheet or nanoribbon FET architectures^{6,33,34}, where optimal channel widths typically fall within tens of nanometers. Unlike traditional FinFETs, whose quantized fin heights limit design flexibility and complicate circuit optimization, GAA structures offer improved scalability and flexible width options.

Compared to silicon-based transistors, 2D semiconductor nanoribbon FETs offer additional advantages from their atomically thin structure, as shown in **Fig. 1a**. Unlike bulk silicon, which exhibits edge states in both channel width and thickness dimensions, 2D nanoribbons primarily present edge states along their lateral borders, owing to naturally passivated surfaces without dangling bonds in the vertical dimension. Additionally, the atomic thinness of 2D materials reduces the proportion of edge states relative to the overall device width, further minimizing detrimental impacts. While graphene nanoribbons still suffer significant edge-related mobility degradation from width scaling³⁵, the corresponding impacts on 2D TMD-based FETs remain less understood. Thus, a detailed exploration of width scaling effects is essential to fully realize the potential of 2D materials in ultra-scaled transistor technologies.

In this study, we uncover the effects of width scaling and demonstrate high-performance 2D monolayer nanoribbon transistors with key dimensions— L_{CH} , L_{CONT} , W_{CH} , and t_{OX} —comparable to state-of-the-art silicon technology nodes. Devices with channel widths narrowed to ~30–40 nm exhibited a 40% enhancement in on-current and a substantial improvement in subthreshold swing, reducing by approximately 30 mV/dec compared

to wider channels. These improvements stem from enhanced electrostatics, as confirmed by Synopsys Sentaurus TCAD simulations, which revealed a stronger electric field at the nanoribbon edges. Photoluminescence measurements further indicated a positive exciton energy shift at the edges, suggesting potential p-doping and depletion region formation. Beyond MoS₂, this nanoribbon architecture was successfully extended to other monolayer TMDs, including WS₂ for n-type FETs and WSe₂ for p-type FETs, demonstrating their suitability for complementary FET (CFET) applications. Additionally, we fabricated arrays of MoS₂ nanoribbon devices with a contact pitch (CP) of 60 nm and an effective oxide thickness (EOT) of ~0.9 nm. These ultra-scaled devices achieved an on-current density (I_{ON}) of ~600 μ A/ μ m at an overdrive voltage (V_{OV}) of 2.5 V, with excellent off-state characteristics, including a subthreshold slope (SS) of ~74 mV/dec and enhancement-mode operation ($V_{TH} > 0$).

Results

Scaling 2D semiconductors toward high-performance transistors

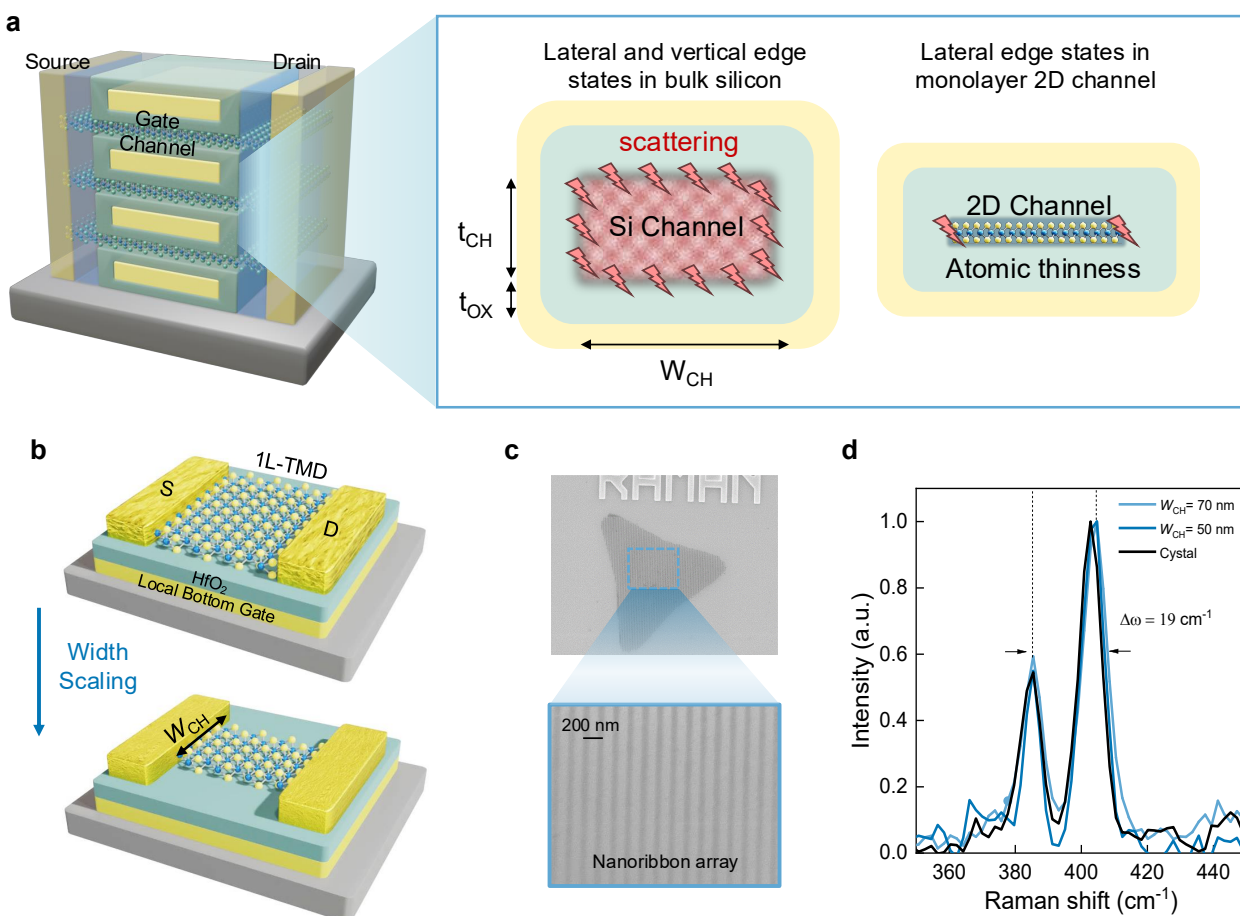


Fig. 1 | Scaled monolayer MoS₂ nanoribbon FETs. **a** Schematic of atomic gate-all-around (Atomic GAA) nanosheet transistors based on 2D monolayer channels and conceptual comparison of edge scattering in bulk silicon vs. 2D monolayer channels. **b** Device schematic of 1L-MoS₂ nanoribbon with Cr/Au local bottom gate (LBG), 3 nm HfO₂ gate dielectric, and Ni source/drain contacts. **c** Scanning electron microscopy (SEM) image of large and uniform nanoribbon array used for **d** Raman spectroscopy. Raman results show preserved E' and A₁' modes post-patterning, confirming minimal disorder from nanoribbon fabrication.

Fig. 1b shows schematic illustrations of monolayer MoS₂ nanoribbon FETs with width scaling to 30-40 nm. Ultra-thin dielectric layers (HfO₂, 3 nm grown at 90°C)²⁰ were employed to enable extreme channel-length scaling, reduce device-to-device variability, and mitigate the influence of the Schottky barrier height at the metal-semiconductor interface. Detailed fabrication procedures are described in the **Methods** section. **Fig. 1c** and **Supplementary Fig. 1** provide representative scanning electron microscopy (SEM) images of fabricated MoS₂ nanoribbons. The images feature both a tapered nanoribbon geometry, specifically designed for systematic studies of width-scaling effects, and uniform large-area nanoribbon arrays intended for optical characterization. Raman spectroscopy was employed to evaluate the effect of the patterning process on crystalline quality (**Fig. 1d**). The absence of detectable shifts in the characteristic E' and A₁' peaks confirms the preservation of MoS₂ crystallinity following the gentle Cl₂/O₂ plasma etching process. This result indicates that nanoribbon patterning down to tens of nanometers does not significantly compromise the crystalline quality, in terms of optical properties. A comprehensive electrical investigation will be discussed in the following session.

Channel width scaling of monolayer TMD nanoribbon FETs

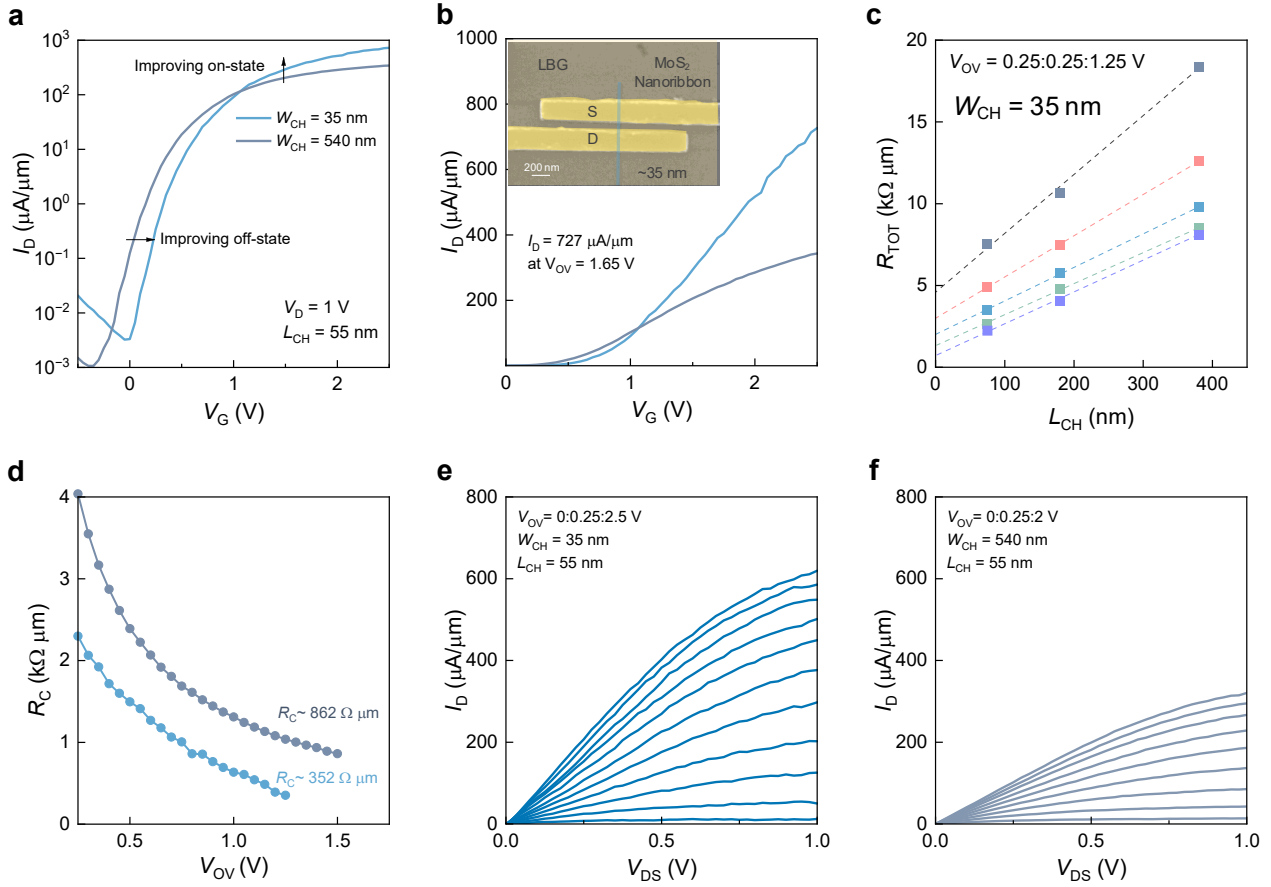


Fig. 2 | Channel width scaling of monolayer MoS₂ nanoribbon FETs with on-current enhancement. **a** Log-scale and **b** linear-scale transfer characteristics (I_D – V_G) for devices with channel widths of 540 nm and 30 nm, showing significant enhancement in both on-state and off-state transistor performance upon width scaling. The inset presents an SEM image of a representative nanoribbon device with a 35 nm channel width and 55 nm channel length. **c** Total resistance (R_{TOT}) as a function of channel length at different overdrive voltage (V_{OV}) from $V_{OV} = 0.25\text{ V}$ to 1.25 V . **d** Contact resistances (R_C) as a function of V_{OV} for wide and narrow nanoribbon devices with channel widths of 540 nm (dark blue) and 35 nm (blue). **e-f** Output characteristics (I_D – V_D) showing the enhanced on-current density in nanoribbon devices.

To investigate the effects of width scaling on monolayer MoS₂ nanoribbon transistors, we fabricated sets of devices with varying channel lengths and widths. **Fig. 2a-b** presents representative log-scale and linear-scale transfer characteristics (I_D – V_G) for two channel widths ($W_{CH} = 540\text{ nm}$ and $W_{CH} = 35\text{ nm}$). The inset image in **Fig. 2b** displays an SEM image of a representative device with $W_{CH} = 35\text{ nm}$ and $L_{CH} = 55\text{ nm}$. **Supplementary Fig. 2** shows the representative SEM images of the precise patterning of MoS₂ nanoribbons. Remarkably,

aggressive scaling of the channel width results in enhanced transistor performance in both the on-state and off-state regimes, achieving a high on-current density (I_{ON}) of $\sim 726 \mu\text{A}/\mu\text{m}$ at $V_D = 1 \text{ V}$ and an overdrive voltage (V_{OV}) of 1.65 V with a steep SS of 94 mv/dec at $V_{DS} = 0.1 \text{ V}$, as shown in **Fig. 2b**. A slight positive shift in the threshold voltage (V_{TH}) and improved SS are observed in the narrow nanoribbon structure, indicating improved gate electrostatics. Such enhanced gate control through width scaling has previously been reported for oxide semiconductors,³⁶ and this study represents the first observation in 2D monolayer MoS₂ devices. This finding contrasts with previous studies of 2D MoS₂, in which width scaling typically degraded device performance.^{37–41} We attribute the observed enhancement here to our gentle etching process, which preserves the crystallinity of the MoS₂, as confirmed by Raman spectroscopy (**Fig. 1d**).

Due to improved electrostatics, the monolayer MoS₂ nanoribbon FETs exhibit exceptionally low contact resistance (R_C), reaching approximately $352 \Omega \cdot \mu\text{m}$ at a scaled overdrive voltage of $V_{OV} = 1.25 \text{ V}$, which is significantly lower than that of wider devices ($R_C \sim 862 \Omega \cdot \mu\text{m}$) as shown in **Fig. 2c-d**. This lower contact resistance in the nanoribbon devices suggests stronger contact gating effects and, consequently, higher carrier density. Moreover, the output characteristics (I_D-V_D) depicted in **Fig. 2e-f** further confirm the improved on-current density of nanoribbon devices. As shown in **Supplementary Fig. 3**, the conductivity mobility (μ_{con}) extracted from transfer length method (TLM) measurements is around $40 \text{ cm}^2 \text{ V}^{-1} \text{ s}^{-1}$.

On the width scaling of 1L-TMD NR FETs

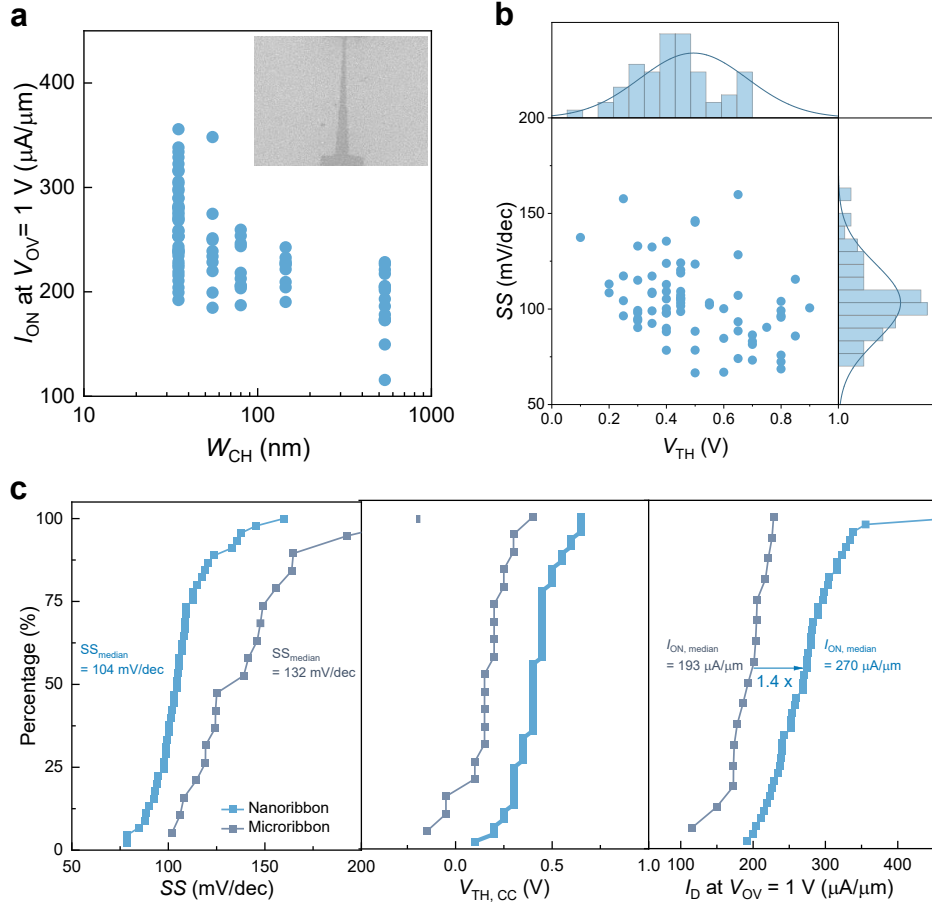


Figure 3. Statistical evaluation of channel width scaling in monolayer MoS₂ nanoribbon FETs. **a**, On-current (I_{ON}) as a function of channel width, measured at $V_D = 1$ V and $V_{OV} = 1$ V. Inset: SEM of a tapered nanoribbon designed for systematic width-dependent studies. **b**, Scatter plots with marginal histograms demonstrating the relationship and variability between threshold voltage (V_{TH}) and subthreshold swing (SS). The statistical analysis indicates low device-to-device variability ($\sigma_{V_t} \sim 0.12$ V, $\sigma_{SS} \sim 16$ mV/dec). **c**, Cumulative distribution functions (CDFs) comparing key performance metrics—SS, V_{TH} , and I_{ON} —between normal-width (540 nm) and aggressively scaled (35 nm) nanoribbon devices. The scaled devices exhibit significantly enhanced median performance, including a ~40% increase in median I_{ON} (from 193 $\mu\text{A}/\mu\text{m}$ to 270 $\mu\text{A}/\mu\text{m}$) at scaled overdrive voltage $V_{OV} = 1$ V and improved median SS (from 132 mV/dec to 104 mV/dec), along with a positive shift in V_{TH} (~0.25 V).

To systematically evaluate the impact and reproducibility of channel width scaling in monolayer MoS₂ nanoribbon FETs, we fabricated and characterized hundreds of devices with varying channel widths and examined the statistics of key device metrics (**Fig. 3a**). A clear upward trend of the on-current (I_{ON}) with decreasing channel width demonstrates enhanced electrostatic control in narrower devices, highlighting the benefit of aggressive width scaling. **Fig. 3b** further elucidates the relationship between threshold voltage (V_{TH}) and subthreshold swing (SS). Devices with positive V_{TH} show lower SS, suggesting that the electric field at the edge enhances electrostatics and that edge-induced charge can modulate V_{TH} . Changes in the charge state near the edge will be investigated directly using photoluminescence, as discussed in the next section. Our statistical analysis reveals low device-to-device variability, with standard deviations of V_{TH} (~0.12 V) and SS (~16 mV/dec), indicating optimized fabrication processes that achieve highly uniform and reliable monolayer MoS₂ nanoribbon transistors.

To quantify variability and compare device performance statistically, we analyzed the cumulative distribution functions (CDFs) of critical metrics (V_{TH} , SS, and I_{ON}) for normal-width (540 nm) and aggressively scaled (35 nm) devices, as shown in **Fig. 3c**. The SS was determined by extracting the minimum slope from the log-scale transfer curves, and $V_{TH,CC}$ was defined at a constant drain current of 100 nA/ μ m at a drain voltage (V_D) of 0.1 V. Note that constant-current extraction is used to evaluate the off-state characteristics.⁴² For a fair comparison of on-state performance, all devices were evaluated at the same overdrive voltage ($V_{OV} = V_{GS} - V_{TH,LIN}$) of 1 V, where $V_{TH,LIN}$ is extracted from transfer characteristics at small V_{DS} by identifying the maximum transconductance and linear extrapolation. Remarkably, the median on-current for the 35 nm-wide devices shows a substantial enhancement (~40%) compared to the wider counterparts, increasing from 193 μ A/ μ m to 270 μ A/ μ m, as illustrated in **Fig. 3c**. Additionally, the median subthreshold swing significantly improves from 132 mV/decade to 104 mV/decade, reflecting the enhanced gate control associated with width scaling. A positive shift in $V_{TH,CC}$ (~0.25 V) is observed, consistent with expectations from improved electrostatics in narrow channels. Notably, despite aggressive scaling, no significant increase in variability of the critical device parameters is observed, highlighting the excellent uniformity and reproducibility of our nanoribbon fabrication approach.

Photoluminescence of monolayer nanoribbon

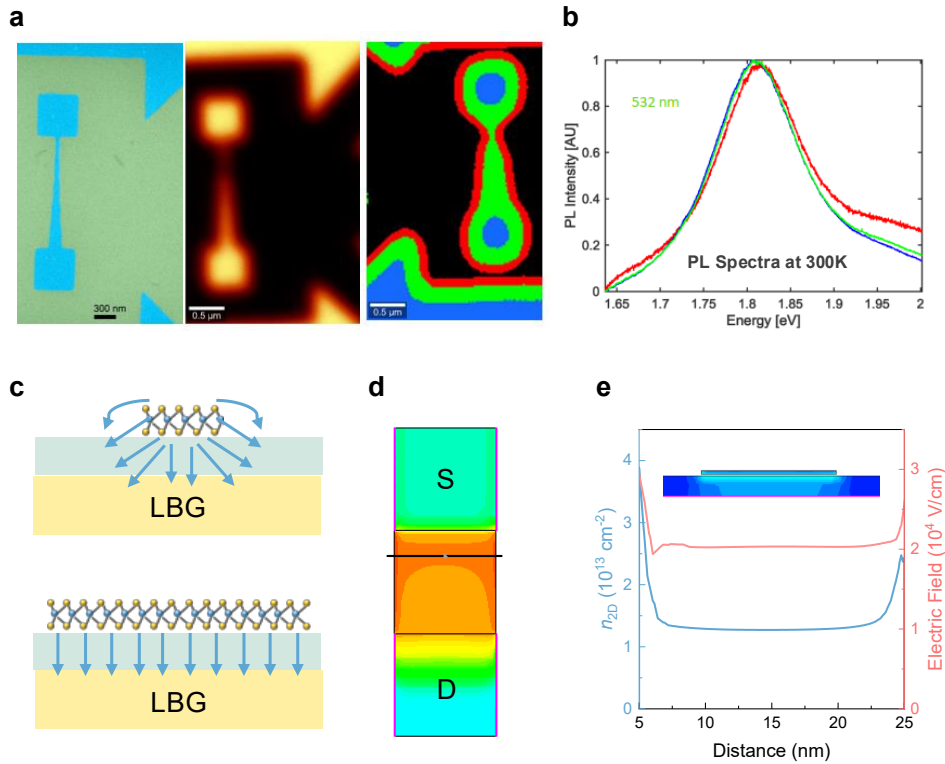


Fig. 4 | Photoluminescence characterization and TCAD simulation of monolayer MoS₂ nanoribbon. **a** A false color SEM of the nanoribbon accompanied by a PL-intensity image of a similar device. PL-spectra were then separated via a K-means clustering process into bulk and edge regions as shown by the third tri-color image from which the average spectra of each region is provided in **b**. **b** Room-temperature PL spectra comparing edge vs. bulk emission. **c** Schematics illustrating enhanced electrostatics due to width scaling and edge field concentration. **d** TCAD-simulated 2D electric field and **e** electron density along the width direction in the on-state ($V_{DS} = 1$ V, $V_G = 3$ V), showing enhanced carrier density at nanoribbon edges.

To investigate the physical mechanisms underlying the observed electrostatic enhancement in monolayer MoS₂ nanoribbon FETs, we conducted detailed photoluminescence (PL) characterization of the patterned nanoribbon edges (**Fig. 4a-b**). The PL spectra revealed a notable positive shift in exciton energy within the nanoribbon edge compared to the bulk region, suggesting potential p-doping and depletion at the nanoribbon edge⁴³. **Supplementary Fig. 4** shows the fitted peak position acquired using 488 and 532 nm laser on a natural and lithographically patterned MoS₂ edge. In all cases, the exciton energy increases upon moving across the

edge. The magnitude of this change is equal irrespective of laser energy or the type of patterning, implying that lithographic patterning and etching does not significantly damage or alter the intrinsic properties of MoS₂ edges.

Interestingly, lithographically patterned edges exhibit slightly higher exciton energy compared to naturally formed edges. We hypothesize this subtle difference arises from near-edge oxygen incorporation introduced during the Cl₂/O₂ plasma etching process. This localized oxygen incorporation could passivate sulfur vacancies through partial oxidation, inducing mild p-type doping—consistent with our observed PL shifts and supported by prior literature. The presence of oxygen passivation effectively removes mid-gap states originating from vacancies, thereby potentially reducing the edge-related mobility degradation and contributing to the observed reduction in contact resistance. Such an effect aligns closely with previously reported improvements observed in oxygen-doped MoS₂ synthesized via direct methods⁴⁴ and oxygen-incorporated MoS₂ from chemical vapor deposition (CVD)⁴⁵.

Fig. 4c presents schematic illustrations of monolayer MoS₂ nanoribbon FETs, emphasizing how aggressive width scaling significantly enhances the gate electric field, thereby improving electrostatic control within these nanoribbon devices. These nanoribbon structures enhance the electric field at the edges and increase carrier densities, while minimally degrading the performance from edge scattering. To gain a deeper understanding, Sentaurus TCAD simulations were performed to quantify and visualize the enhanced electrostatic effects that contribute to current improvement and lower contact resistance (**Fig. 4d-e**). The simulated two-dimensional carrier density (n_{2D}) and lateral electric field distributions clearly reveal intensified edge fields and modified carrier densities near the nanoribbon edges. Collectively, these findings substantiate the role of controlled edge doping and electrostatic modulation as key factors driving performance enhancement in aggressively scaled MoS₂ nanoribbon devices.

High-performance monolayer nanoribbon WSe₂ p-FETs and WS₂ n-FETs

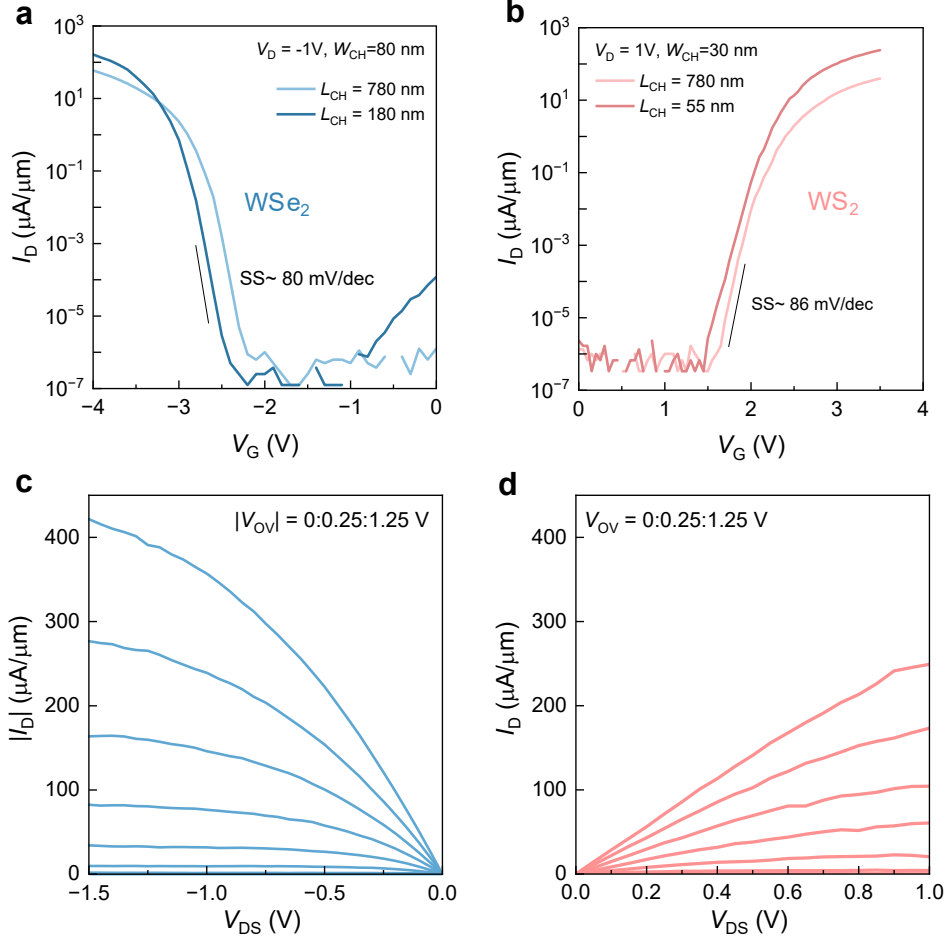


Fig. 5 | Electrical characteristics and statistics of NO-doped 1L-WSe₂ NR p-FETs. a Transfer (I_D – V_G) and **c** output (I_D – V_D) characteristics of NO-doped monolayer WSe₂ p-FETs. **b** Transfer and **d** output characteristics of monolayer WS₂ n-FETs. Both devices show strong performance with high on-current and excellent subthreshold behavior, validating the scalability of nanoribbon FETs across different TMDs.

To demonstrate the versatility and robustness of channel-width scaling in monolayer nanoribbon field-effect transistors, we fabricated high-performance p-type WSe₂ and n-type WS₂ transistors using a fabrication approach similar to that described previously for MoS₂. Unlike MoS₂, 6 nm HfO₂ was grown at 200 °C to improve film quality and the dielectric constant⁴⁶. In particular, nitric oxide (NO) doping was used in WSe₂ devices to significantly enhance hole injection and reduce contact resistance^{24,28,46,47}. The resulting WSe₂ p-FETs (**Fig. 5a,c**) exhibit excellent device characteristics, including a subthreshold swing (SS) of approximately 80 mV/dec and a high on-current of around 400 μ A/ μ m for a channel length (L_{CH}) of 380 nm. Despite the

notable enhancement provided by NO doping, the threshold voltage (V_{TH}) remains negative, highlighting the necessity for additional threshold voltage tuning, particularly for aggressively scaled dimensions.

In parallel, WS_2 n-FETs (Fig. 5b,d) were fabricated and similarly characterized, demonstrating comparable transistor performance. In contrast to MoS_2 -based n-FETs, WS_2 devices exhibit a more positive threshold voltage. This positive shift can be attributed to differences in the affinity of the channel relative to the gate metal and variations in intrinsic defect density, such as sulfur vacancy concentrations. Notably, the WS_2 nanoribbon transistors achieve robust performance with an impressive on-current of approximately $200 \mu A/\mu m$ even under relatively small overdrive voltages ($V_{ov}=1.25$ V). These results underscore the broad applicability and effectiveness of nanoribbon dimensional scaling combined with careful doping and material selection for advancing the performance of 2D monolayer transistors.

Extremely scaled monolayer nanoribbon FETs

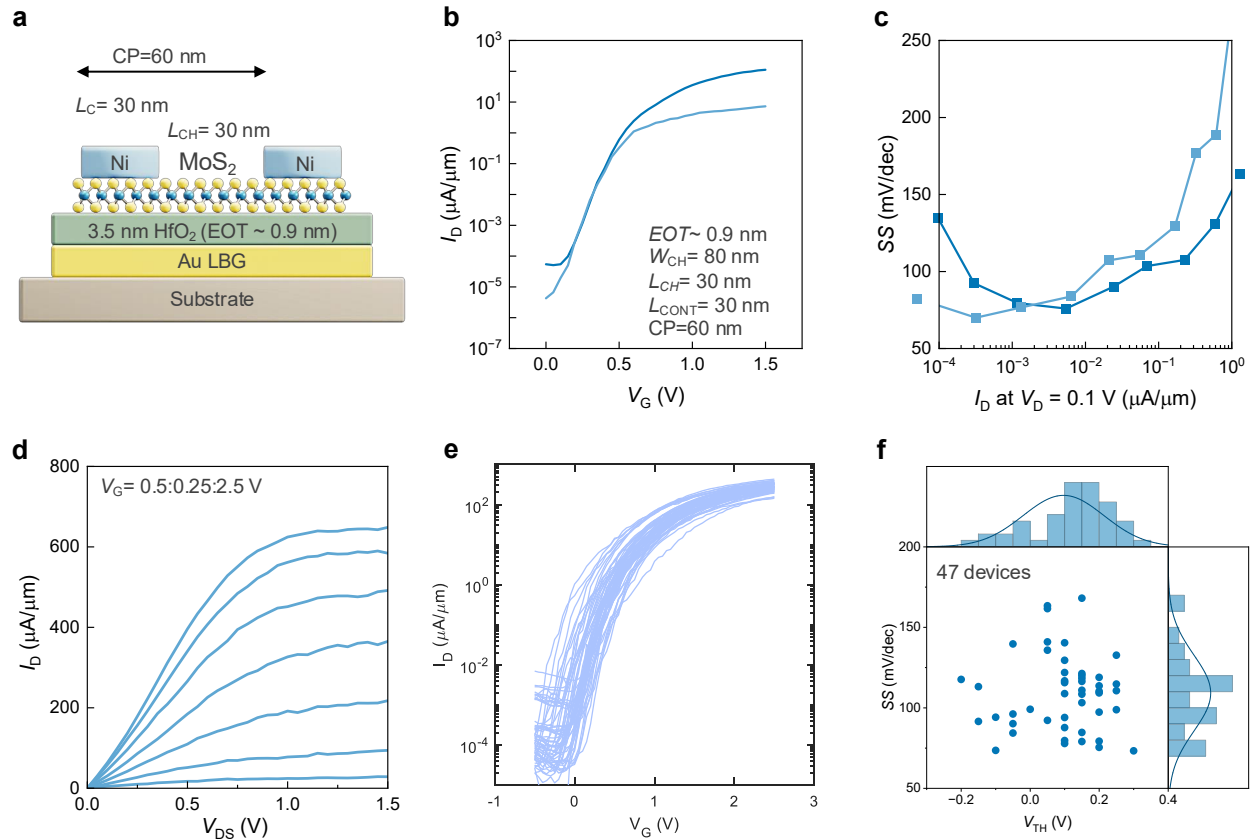


Figure 6. Ultra-scaled monolayer MoS_2 nanoribbon FETs. **a** Cross-sectional schematic showing device structure with $CP = 60$ nm, $L_{CH} = 30$ nm, $L_C = 30$ nm, and $EOT \approx 0.9$ nm. **b** Log-scale I_D-V_G characteristics of

representative devices. **c** Extracted subthreshold swing (SS) as a function of I_D . **d** Output characteristics (I_D – V_D) demonstrating well-behaved saturation. **e** Statistical I_D – V_G curves across the device set. **f** Scatter plot with histograms for V_{TH} and SS from 47 devices. No strong correlation is observed.

In addition to width scaling, reducing device dimensions in the length direction—including both channel length (L_{CH}) and contact length (L_C)—and in thickness (oxide) is crucial for evaluating the ultimate scalability and performance potential of 2D transistors. Here, we demonstrate ultra-scaled monolayer MoS₂ FETs with critical dimensions: contact pitch (CP) = 60 nm, channel width (W_{CH}) = 80 nm, equivalent oxide thickness (EOT) \approx 0.9 nm with 3 nm HfO₂, and channel/contact lengths of 30 nm (Fig. 6a), making these devices among one of the smallest reported 2D transistors to date. Remarkably, despite their aggressively scaled dimensions, these devices exhibit excellent electrical performance in both on-state and off-state regimes, achieving an on/off current ratio exceeding 10⁶ at a modest gate bias of 1.5 V.

The representative device exhibits a subthreshold swing (SS) as low as 74 mV/dec (Fig. 6b-c), emphasizing superior gate electrostatics and minimal short-channel effects (SCEs), with negligible drain-induced barrier lowering (DIBL) observed. In terms of on-state performance, the device delivers a high saturation current of approximately 600 μ A/ μ m at a drain bias (V_{DS}) of 1 V and a gate overdrive (V_{ov}) of 2.5 V, with well-defined saturation behavior indicating minimal SCEs (Fig. 6d). However, we observe a slight degradation in on-current when the contact length is aggressively reduced from 70 nm to 30 nm, likely due to an increase in contact resistance likely associated with current crowding (as illustrated in Supplementary Fig. 5). Further improving contact resistance by semimetal contact is need to further scale contact length,^{19,48} which is out of the scope of this study.

Statistical analysis of a set of 47 devices reveals that the mean subthreshold swing is around 110 mV/dec with a standard deviation of 24 mV/dec, and the mean threshold voltage (V_{TH}) is approximately 0.12 V with a standard deviation of 0.1 V (Fig. 6e-f). This low variability can be primarily attributed to the ultra-scaled, high-quality dielectric (HfO₂, EOT \approx 0.9 nm) employed in this study, along with the excellent uniformity of the monolayer MoS₂ channel material. The device performance demonstrated here can be further enhanced through

contact engineering, such as using semimetal contacts to lower contact resistance, further thinning the gate dielectric, or employing a double-gate architecture, all of which represent future research directions.

Discussion

In summary, we demonstrated significant performance enhancement in aggressively scaled monolayer TMD nanoribbon transistors, including MoS₂, WS₂, and WSe₂. By reducing channel width and length and employing ultra-thin gate dielectrics, we achieved excellent electrostatic control, minimal short-channel effects, and low device-to-device variability. Detailed spectroscopic analyses confirmed preserved crystallinity and indicated beneficial edge doping effects. Ultra-scaled MoS₂ transistors with a contact pitch of 60 nm can achieve a high on-current of approximately 600 μ A/ μ m and a subthreshold swing of about 74 mV/dec. These results highlight the potential of 2D monolayer semiconductors for future ultra-scaled electronics, particularly in complementary field-effect transistor (CFET) technologies utilizing gate-all-around nanoribbon architectures.

Methods

Materials

2-inch MBE-grown monolayer MoS₂ and WS₂ films were purchased from 2D Semiconductor Co., Ltd.

2-inch CVD-grown monolayer MoS₂ and WSe₂ films were provided by Nexstrom Pte. Ltd.

Raman characterization

Raman spectroscopy was performed using a Thermo Scientific DXR3xi Raman Imaging Microscope with a 532 nm green laser, producing a spot size of approximately 1 μ m. Each Raman mapping was conducted over \sim 10 μ m² on a CVD-grown 1L-MoS₂ film from 2D Semiconductor Co., Ltd.

Photoluminescence characterization

Two separate measurements were performed each using an alpha300R WitecSpectral imaging system. First, PL images were acquired on the edge of the monolayer MoS₂ test structures using 1 mW of 488 and 532 nm light focused on an approximately diffraction limited spot-size with a 100X/0.95 NA objective in a backscattering arrangement. Scattered light was dispersed with a Czerny-Turner spectrometer using a 300 L/mm grating resulting in a spectral accuracy of $< 1.5 \text{ cm}^{-1}$ ($< 0.1 \text{ nm}$ or $< 5 \text{ meV}$). Spectral acquisitions were acquired over a 5x5 μ m area with acquisitions every 25 nm.

Device fabrication

First, we pattern a Cr (3 nm) / Au (12 nm) local bottom gate (LBG), followed by ALD deposition of 3 nm ALD HfO₂ at 90°C ($\kappa \sim 10$) for MoS₂ nanoribbon,²⁰ 6 nm HfO₂ at 200°C ($\kappa \sim 15$) for WS₂ and WSe₂ nanoribbon,⁴⁶ and 3.5 nm HfO₂ at 200°C ($\kappa \sim 15$) for extremely scaled MoS₂ devices, which serves as the bottom gate dielectric. Subsequently, wafer-grown 1L-MoS₂ films are wet transferred onto the LBG substrate. We then pattern the MoS₂ channel by reactive ion etching using Cl₂/O₂. Ni source/drain (S/D) contacts with different W_{CH} , L_{CH} , and L_{CONT} are patterned using e-beam lithography and e-beam evaporation.

Electrical characterization

The electrical characterization under vacuum ($\sim 1 \times 10^{-5}$ torr) was performed using a Keysight 4156C Precision Semiconductor Parameter Analyzer.

Data Availability

Relevant data supporting the key findings of this study are available within the article and the Supplementary Information file. All raw data generated during the current study are available from the corresponding authors upon request.

References

1. Salahuddin, S., Ni, K. & Datta, S. The era of hyper-scaling in electronics. *Nat. Electron.* **1**, 442–450 (2018).
2. Lee, M. L., Fitzgerald, E. A., Bulsara, M. T., Currie, M. T. & Lochtefeld, A. Strained Si, SiGe, and Ge channels for high-mobility metal-oxide-semiconductor field-effect transistors. *J. Appl. Phys.* **97**, 011101 (2005).
3. Chau, R. *et al.* High-k/Metal-Gate Stack and Its MOSFET Characteristics. *IEEE Electron Device Lett.* **25**, 408–410 (2004).
4. Chenming Hu *et al.* FinFET-a self-aligned double-gate MOSFET scalable to 20 nm. *IEEE Trans. Electron Devices* **47**, 2320–2325 (2000).

5. Colinge, J.-P. *et al.* Nanowire transistors without junctions. *Nat. Nanotechnol.* **5**, 225–229 (2010).
6. Loubet, N. *et al.* Stacked nanosheet gate-all-around transistor to enable scaling beyond FinFET. in *2017 Symposium on VLSI Technology* T230–T231 (IEEE, Kyoto, Japan, 2017). doi:10.23919/VLSIT.2017.7998183.
7. Agrawal, A. *et al.* Silicon RibbonFET CMOS at 6nm Gate Length. in *2024 IEEE International Electron Devices Meeting (IEDM)* 1–4 (2024). doi:10.1109/IEDM50854.2024.10873367.
8. Huang, C. Y. *et al.* 3-D Self-aligned Stacked NMOS-on-PMOS Nanoribbon Transistors for Continued Moore’s Law Scaling. in *2020 IEEE International Electron Devices Meeting (IEDM)* 20.6.1-20.6.4 (IEEE, San Francisco, CA, USA, 2020). doi:10.1109/IEDM13553.2020.9372066.
9. Chhowalla, M., Jena, D. & Zhang, H. Two-dimensional semiconductors for transistors. *Nat. Rev. Mater.* **1**, 16052 (2016).
10. Akinwande, D. *et al.* Graphene and two-dimensional materials for silicon technology. *Nature* **573**, 507–518 (2019).
11. Liu, C. *et al.* Two-dimensional materials for next-generation computing technologies. *Nat. Nanotechnol.* **15**, 545–557 (2020).
12. Liu, Y. *et al.* Promises and prospects of two-dimensional transistors. *Nature* **591**, 43–53 (2021).
13. Zhu, K. *et al.* The development of integrated circuits based on two-dimensional materials. *Nat. Electron.* **4**, 775–785 (2021).

14. Das, S. *et al.* Transistors based on two-dimensional materials for future integrated circuits. *Nat. Electron.* **4**, 786–799 (2021).

15. Jiang, J., Xu, L., Qiu, C. & Peng, L.-M. Ballistic two-dimensional InSe transistors. *Nature* **616**, 470–475 (2023).

16. Desai, S. B. *et al.* MoS₂ transistors with 1-nanometer gate lengths. *Science* **354**, 99–102 (2016).

17. Shen, P. C. *et al.* Ultralow contact resistance between semimetal and monolayer semiconductors. *Nature* **593**, 211–217 (2021).

18. Lan, H.-Y., Appenzeller, J. & Chen, Z. Dielectric Interface Engineering for High-Performance Monolayer MoS₂ Transistors via hBN Interfacial Layer and Ta Seeding. in *2022 International Electron Devices Meeting (IEDM)* 7.7.1-7.7.4 (IEEE, San Francisco, CA, USA, 2022).
doi:10.1109/IEDM45625.2022.10019439.

19. Li, W. *et al.* Approaching the quantum limit in two-dimensional semiconductor contacts. *Nature* **613**, 274–279 (2023).

20. Lan, H.-Y., Oleshko, V. P., Davydov, A. V., Appenzeller, J. & Chen, Z. Dielectric Interface Engineering for High-Performance Monolayer MoS₂ Transistors via TaO_x Interfacial Layer. *IEEE Trans. Electron Devices* **70**, 2067–2074 (2023).

21. Jiang, J. *et al.* Yttrium-doping-induced metallization of molybdenum disulfide for ohmic contacts in two-dimensional transistors. *Nat. Electron.* **7**, 545–556 (2024).

22. Sun, Z. *et al.* Low Contact Resistance on Monolayer MoS₂ Field-Effect Transistors Achieved by CMOS-Compatible Metal Contacts. *ACS Nano* **18**, 22444–22453 (2024).

23. O'Brien, K. P. *et al.* Advancing 2D Monolayer CMOS Through Contact, Channel and Interface Engineering. in *2021 IEEE International Electron Devices Meeting (IEDM)* 7.1.1-7.1.4 (IEEE, San Francisco, CA, USA, 2021). doi:10.1109/IEDM19574.2021.9720651.

24. Chiang, C.-C., Lan, H.-Y., Pang, C.-S., Appenzeller, J. & Chen, Z. Air-Stable P-Doping in Record High-Performance Monolayer WSe₂ Devices. *IEEE Electron Device Lett.* **43**, 319–322 (2022).

25. Chou, A.-S. *et al.* High-Performance Monolayer WSe₂ p/n FETs via Antimony-Platinum Modulated Contact Technology towards 2D CMOS Electronics. in *2022 International Electron Devices Meeting (IEDM)* 7.2.1-7.2.4 (IEEE, San Francisco, CA, USA, 2022). doi:10.1109/IEDM45625.2022.10019491.

26. Wu, R. *et al.* Bilayer tungsten diselenide transistors with on-state currents exceeding 1.5 milliamperes per micrometre. *Nat. Electron.* **5**, 497–504 (2022).

27. Xiong, X. *et al.* Top-Gate CVD WSe₂ pFETs with Record-High $I_d \sim 594 \mu\text{A}/\mu\text{m}$, $G_m \sim 244 \mu\text{S}/\mu\text{m}$ and WSe₂/MoS₂ CFET based Half-adder Circuit Using Monolithic 3D Integration. in *2022 International Electron Devices Meeting (IEDM)* 20.6.1-20.6.4 (IEEE, San Francisco, CA, USA, 2022). doi:10.1109/IEDM45625.2022.10019476.

28. Lan, H.-Y., Tripathi, R., Liu, X., Appenzeller, J. & Chen, Z. Wafer-scale CVD Monolayer WSe₂ p-FETs with Record-high $727 \mu\text{A}/\mu\text{m} I_{ON}$ and $490 \mu\text{S}/\mu\text{m} g_{max}$ via Hybrid Charge Transfer and Molecular Doping.

in *2023 International Electron Devices Meeting (IEDM)* 1–4 (IEEE, San Francisco, CA, USA, 2023). doi:10.1109/IEDM45741.2023.10413736.

29. Lan, H.-Y. *et al.* Stable Nitric Oxide Doping in Monolayer WSe₂ for High-Performance P-type Transistors. Preprint at <https://doi.org/10.21203/rs.3.rs-4916442/v1> (2024).

30. Mortelmans, W. *et al.* Record Performance in GAA 2D NMOS and PMOS Using Monolayer MoS₂ and WSe₂ with Scaled Contact and Gate Length. in *2024 IEEE Symposium on VLSI Technology and Circuits (VLSI Technology and Circuits)* 1–2 (IEEE, Honolulu, HI, USA, 2024). doi:10.1109/VLSITechnologyandCir46783.2024.10631395.

31. Gilardi, C. *et al.* Extended Scale Length Theory Targeting Low-Dimensional FETs for Carbon Nanotube FET Digital Logic Design-Technology Co-optimization. in *2021 IEEE International Electron Devices Meeting (IEDM)* 27.3.1-27.3.4 (2021). doi:10.1109/IEDM19574.2021.9720672.

32. Gilardi, C. *et al.* Extended Scale Length Theory for Low-Dimensional Field-Effect Transistors. *IEEE Trans. Electron Devices* **69**, 5302–5309 (2022).

33. Nagy, D. *et al.* FinFET Versus Gate-All-Around Nanowire FET: Performance, Scaling, and Variability. *IEEE J. Electron Devices Soc.* **6**, 332–340 (2018).

34. Cao, W. *et al.* The future transistors. *Nature* **620**, 501–515 (2023).

35. Yinxiao, Y. & Murali, R. Impact of Size Effect on Graphene Nanoribbon Transport. *IEEE Electron Device Lett.* **31**, 237–239 (2010).

36. Zhang, Z. *et al.* A Gate-All-Around inO Nanoribbon FET With Near 20 mA/m Drain Current <sub/> <sub/> <sub/>. *IEEE Electron Device Lett.* **43**, 1905–1908 (2022).

37. Chen, S. *et al.* Monolayer MoS₂ Nanoribbon Transistors Fabricated by Scanning Probe Lithography. *Nano Lett.* **19**, 2092–2098 (2019).

38. Kotekar-Patil, D., Deng, J., Wong, S. L., Lau, C. S. & Goh, K. E. J. Single layer MoS₂ nanoribbon field effect transistor. *Appl. Phys. Lett.* **114**, (2019).

39. Duan, X. *et al.* MoS₂ Nanoribbon Transistor for Logic Electronics. *IEEE Trans. Electron Devices* 1–6 (2022) doi:10.1109/TED.2022.3164859.

40. Chen, S., Zhang, Y., King, W. P., Bashir, R. & Van Der Zande, A. M. Edge-Passivated Monolayer WSe₂ Nanoribbon Transistors. *Adv. Mater.* 2313694 (2024) doi:10.1002/adma.202313694.

41. Hoque, Md. A. *et al.* Ultranarrow Semiconductor WS₂ Nanoribbon Field-Effect Transistors. *Nano Lett.* **25**, 1750–1757 (2025).

42. Arutchelvan, G. *et al.* Impact of device scaling on the electrical properties of MoS₂ field-effect transistors. *Sci. Rep.* **11**, 6610 (2021).

43. Wang, K., Taniguchi, T., Watanabe, K. & Xue, J. Natural p–n Junctions at the MoS₂ Flake Edges. *ACS Appl. Mater. Interfaces* **14**, 39039–39045 (2022).

44. Tang, J. *et al.* In Situ Oxygen Doping of Monolayer MoS₂ for Novel Electronics. *Small* **16**, 2004276 (2020).

45. Shen, P.-C. *et al.* Healing of donor defect states in monolayer molybdenum disulfide using oxygen-incorporated chemical vapour deposition. *Nat. Electron.* <https://doi.org/10.1038/s41928-021-00685-8> (2021) doi:10.1038/s41928-021-00685-8.
46. Lan, H.-Y. *et al.* Uncovering the doping mechanism of nitric oxide in high-performance P-type WSe₂ transistors. *Nat. Commun.* **16**, 4160 (2025).
47. Lan, H.-Y. *et al.* Improved Hysteresis of High-Performance p-Type WSe₂ Transistors with Native Oxide WO_x Interfacial Layer. *Nano Lett.* **25**, 5616–5623 (2025).
48. Wu, W.-C. *et al.* On the Extreme Scaling of Transistors with Monolayer MoS₂ Channel. in *2024 IEEE Symposium on VLSI Technology and Circuits (VLSI Technology and Circuits) 1–2* (IEEE, Honolulu, HI, USA, 2024). doi:10.1109/VLSITechnologyandCir46783.2024.10631401.

Acknowledgements

This work was supported in part by the Semiconductor Research Corporation (SRC) and National Institute of Standards and Technology (NIST) through the NEW LIMITS Center under Award 70NANB17H041. This work was conducted using the facilities at the Birck Nanotechnology Center.

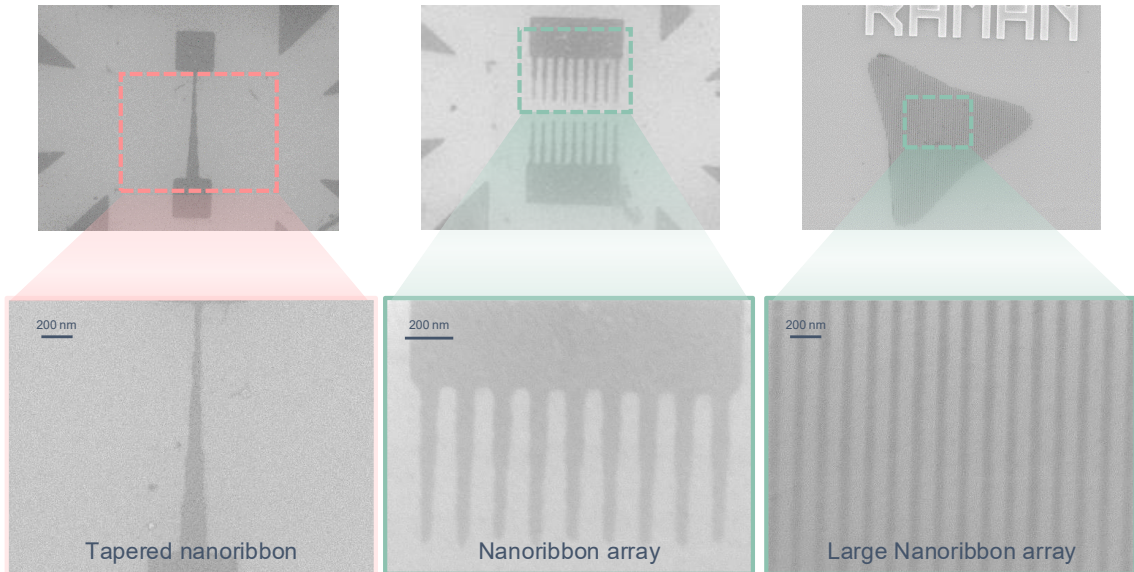
Author Contributions

H.-Y. L. proposed the original idea. Z. C. and J. A. supervised the project. H.-Y. L. performed device fabrication, characterization, simulation, and data analysis with the help of S.-H. Y., Y. Cho, J. Cai, and Z. Sun. C. Li. and L.-Y. H. grew the 2D materials with the input from Y. Wan and L.-J. L.. T. B. performed photoluminescence and data analysis. H.-Y. L. wrote the first draft of the manuscript, and all authors discussed and revised the final manuscript.

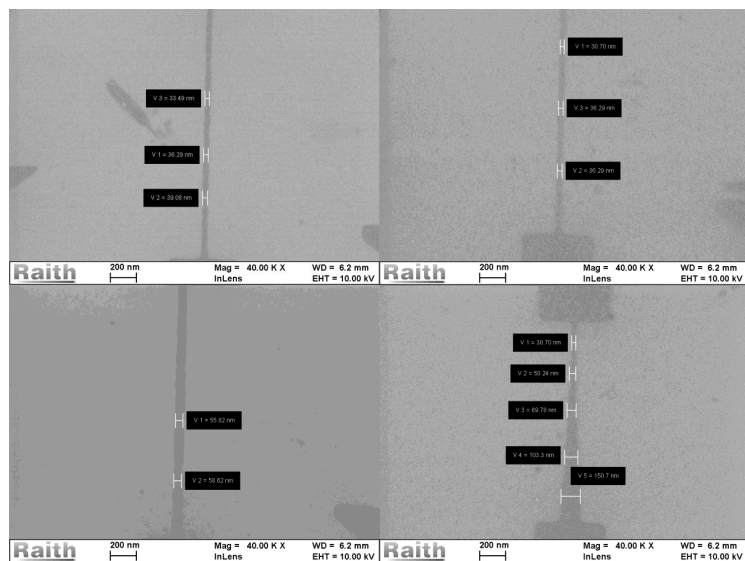
Competing Interests

The authors declare no competing financial interests.

Supplementary Figures

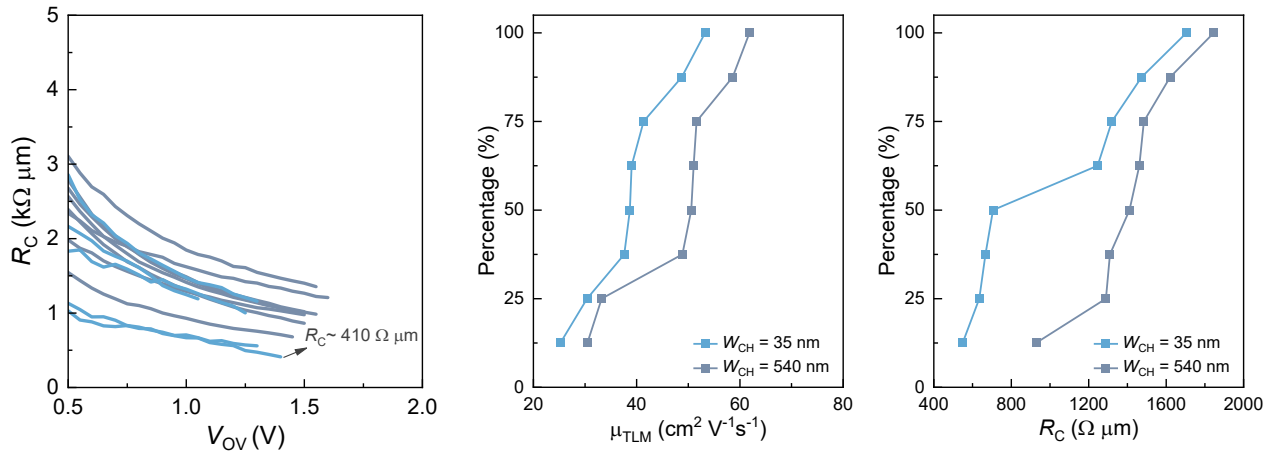


Supplementary Fig. 1 | Nanoribbon structure. SEM images of monolayer MoS₂ nanoribbon. **a** SEM of a tapered nanoribbon designed for systematic width-dependent studies. **b-c** SEM of nanoribbon arrays intended for electrical and large-scale optical characterization. Scale bar: 200 nm.

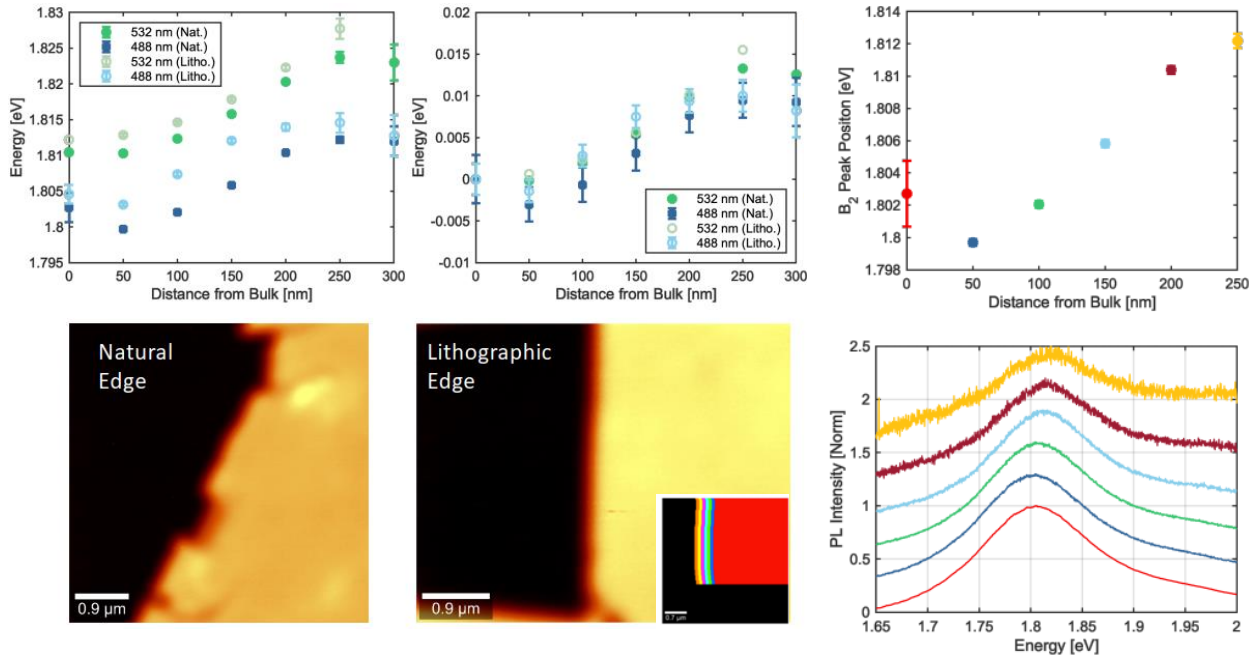


Supplementary Fig. 2 | High-resolution SEM images showing precise nanoribbon patterning for monolayer MoS₂ devices. Scale bars: 200 nm.

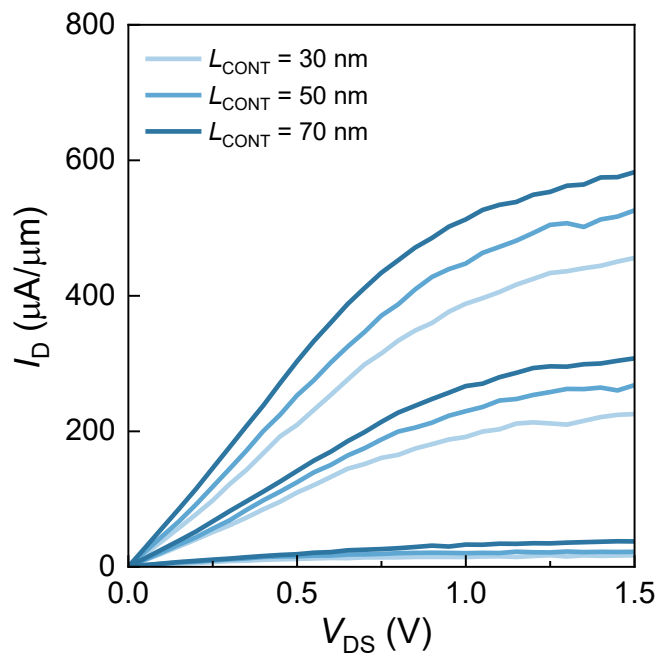
6



Supplementary Fig. 3 | Statistical analysis of contact resistance (R_C) and variability across nanoribbon devices. **a** R_C versus V_{OV} extracted from multiple TLM structures for wide and narrow nanoribbon devices with channel widths of 540 nm (dark blue) and 30 nm (blue). **b-c** Cumulative distribution functions (CDFs) of conductivity mobility (μ_{TLM}) and R_C . Contact resistance shows improvement from nanoribbon devices due to better electrostatics.

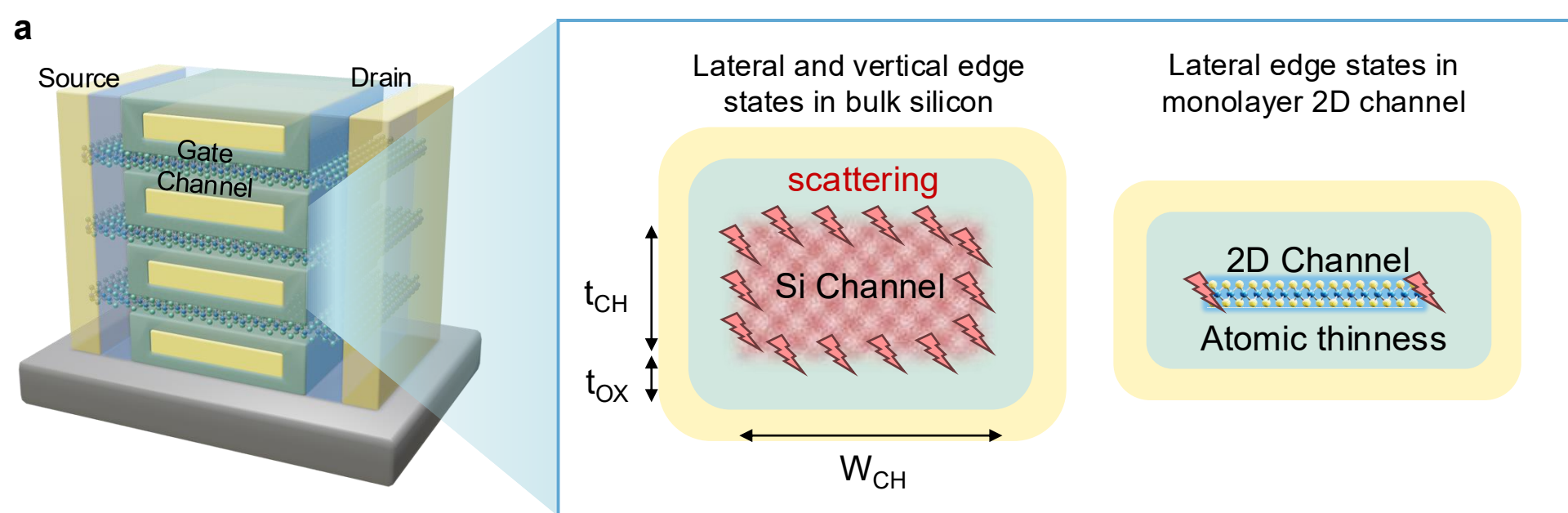


Supplementary Fig. 4 | Photoluminescence comparison of natural edge and lithographic edge. **a** Peak energy shift as a function of distance from the bulk. **b** Relative blueshift trend consistency across laser wavelengths. **c** Intensity mapping images of natural and lithographic edges. **d** PL spectra vs. distance showing edge-related energy shifts.

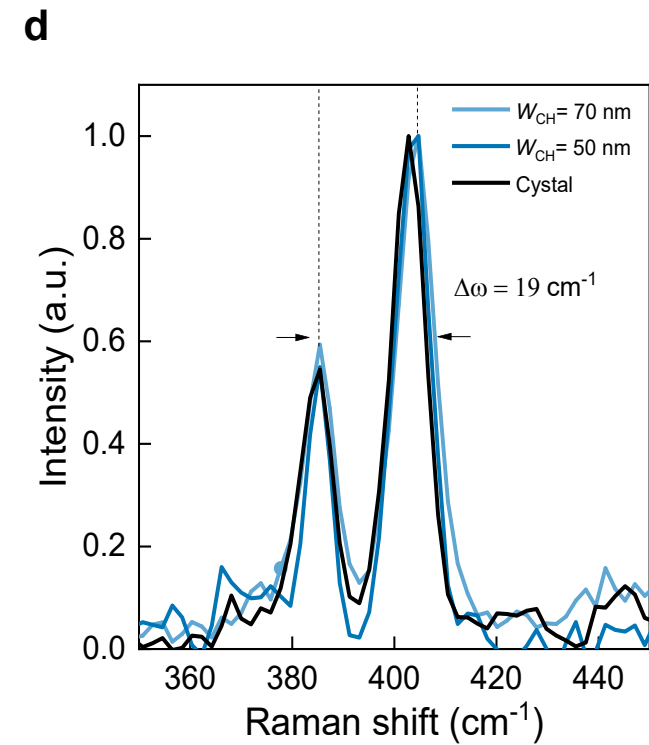
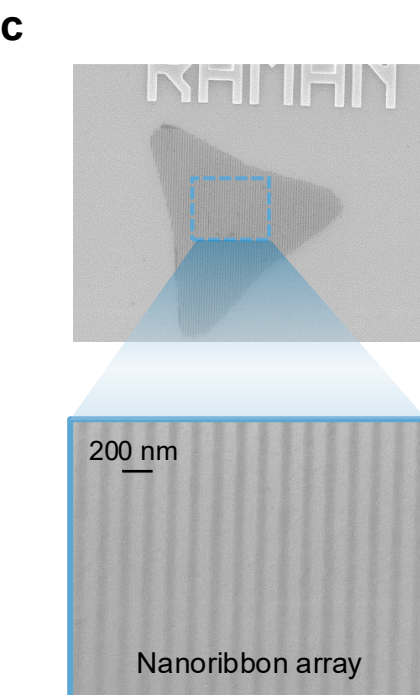
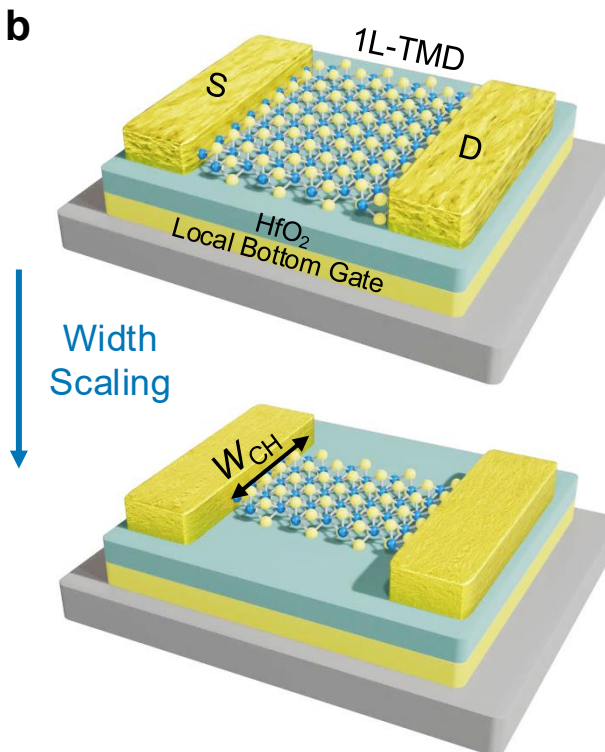
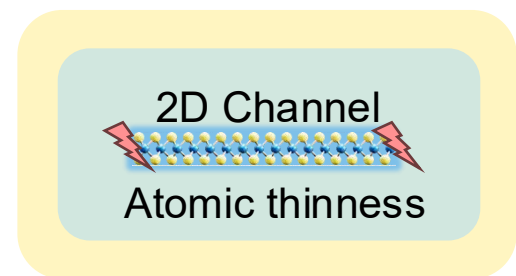


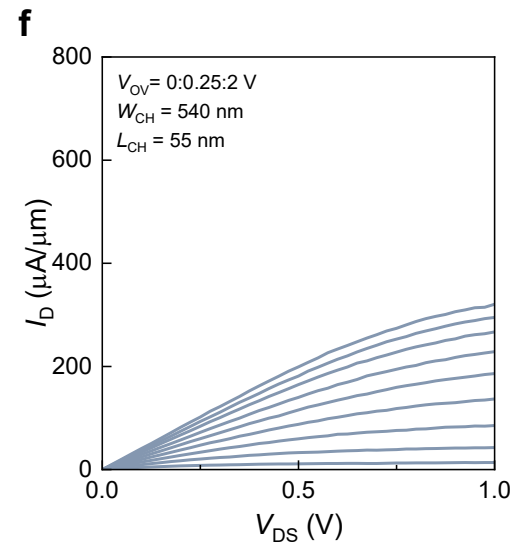
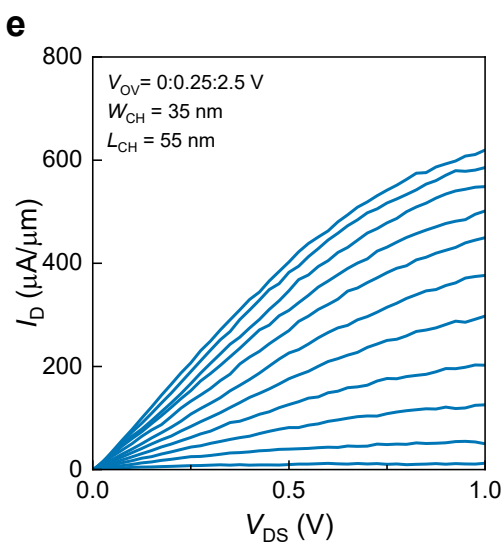
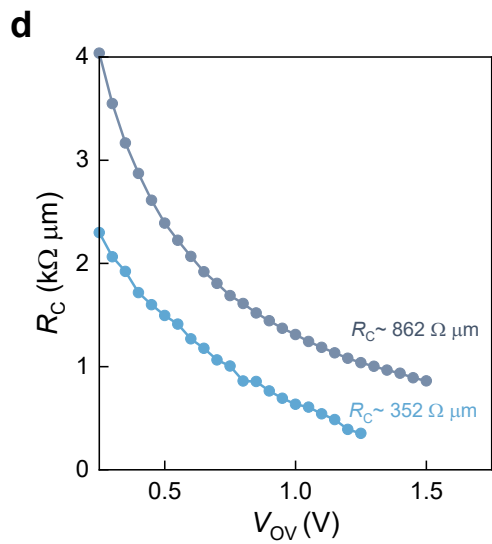
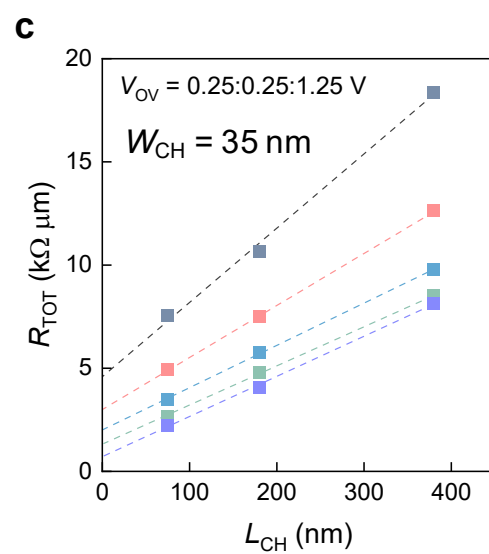
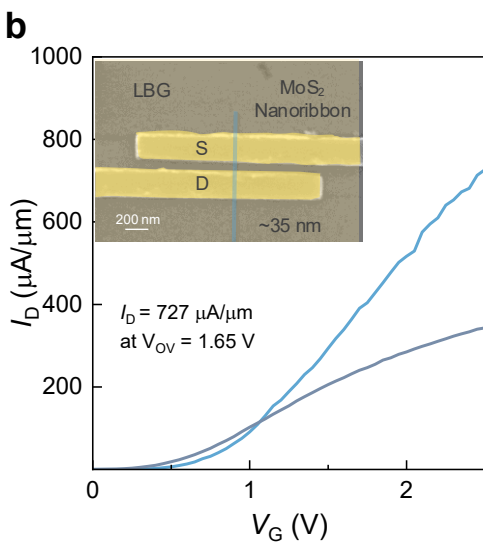
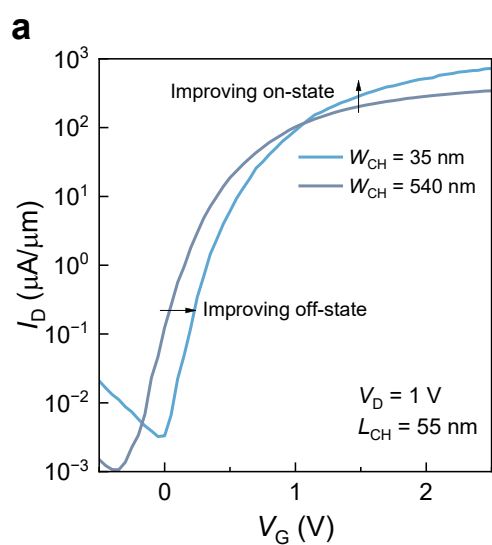
Supplementary Fig. 5 | Effect of contact length scaling on 2D monolayer MoS₂ nanoribbon transistors.

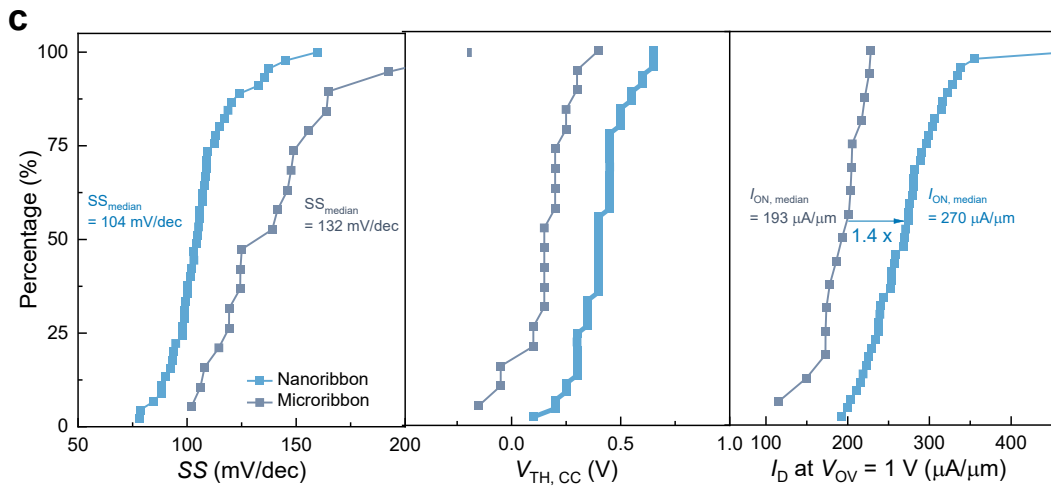
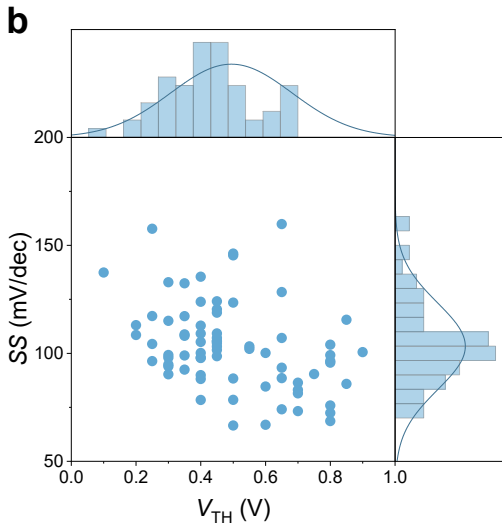
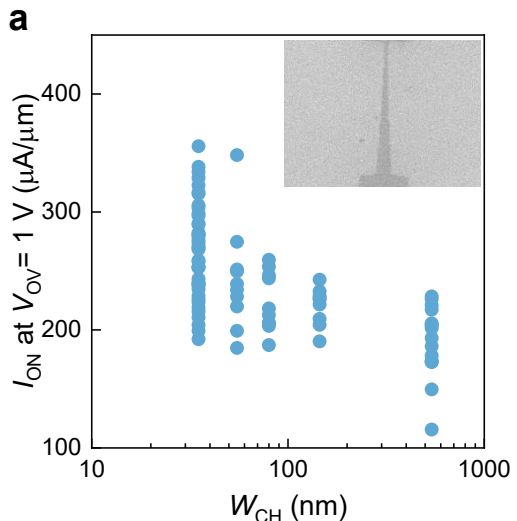
Output characteristics for different contact lengths (L_{CONT}) showing current degradation at $L_{\text{CONT}} = 30$ nm due to increased contact resistance and current crowding effects.

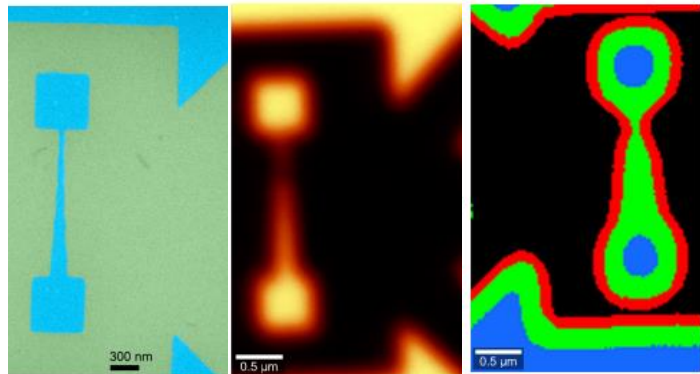
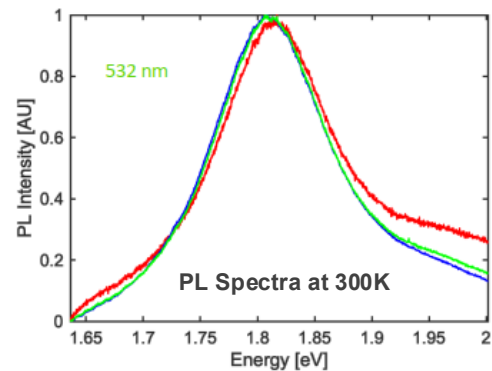
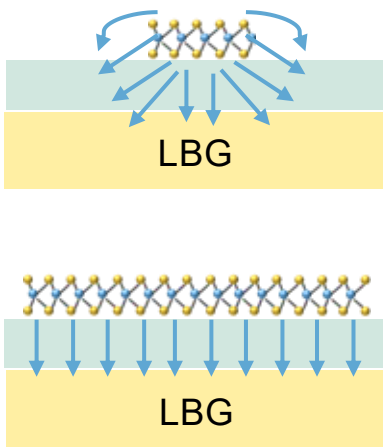
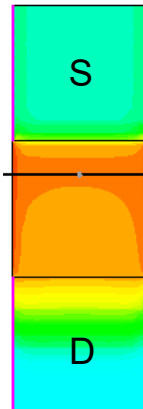
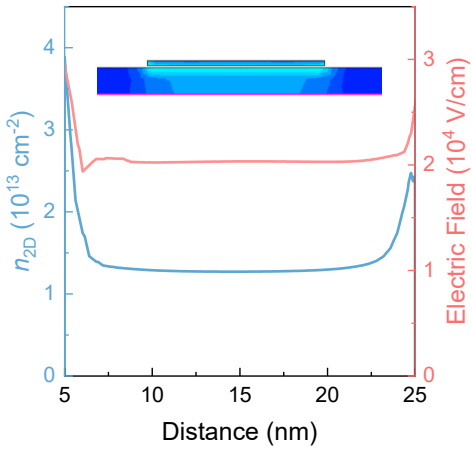


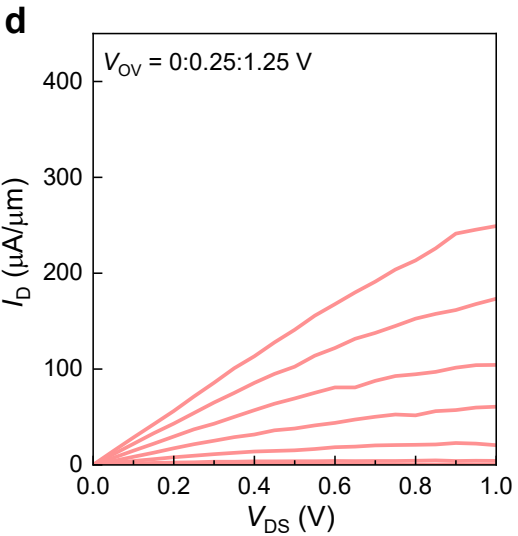
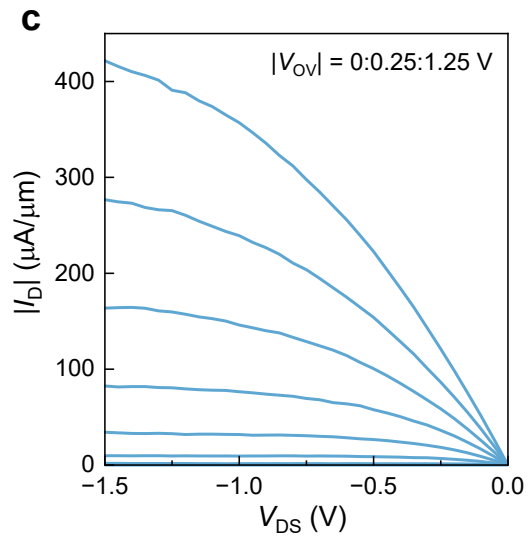
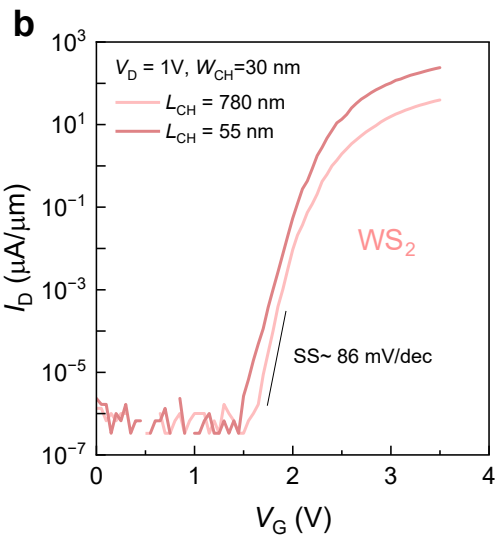
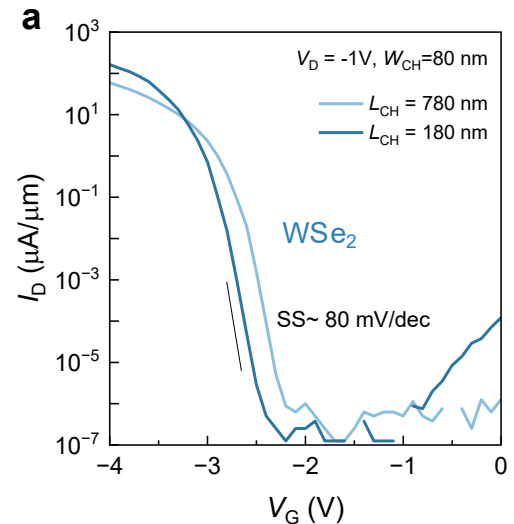
Lateral edge states in monolayer 2D channel

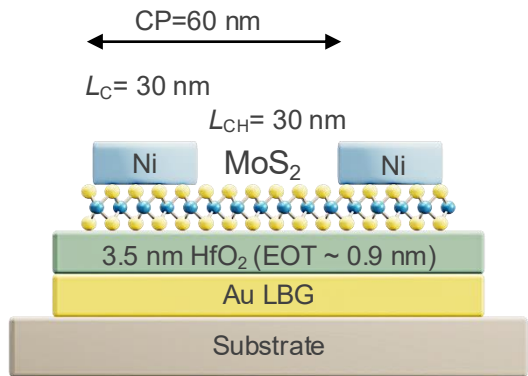
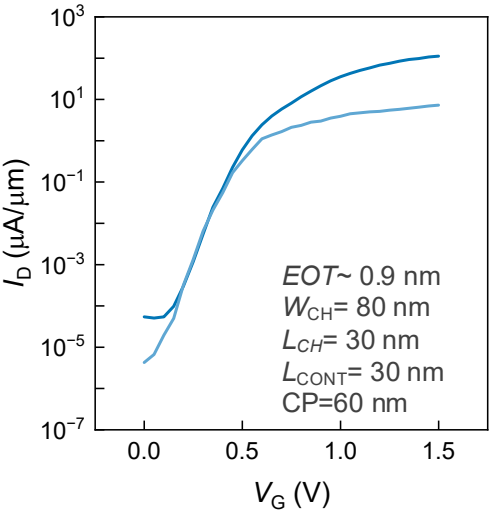
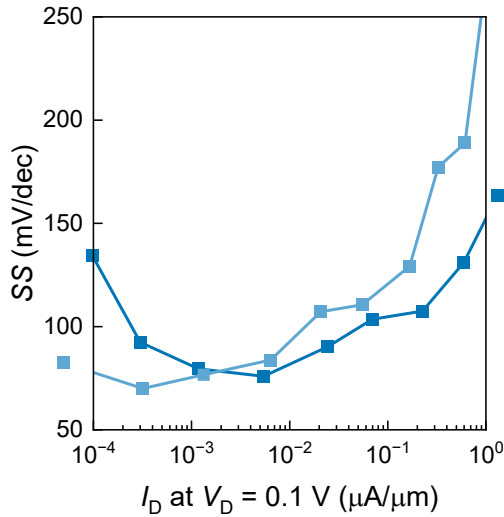
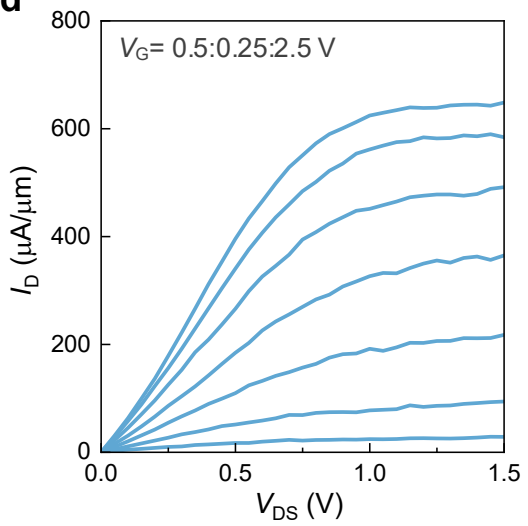
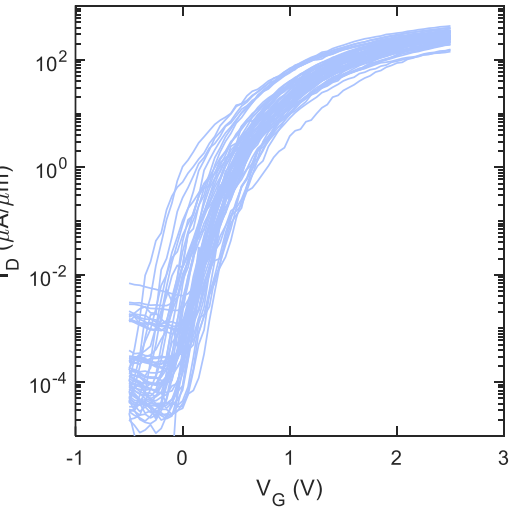






a**b****c****d****e**



a**b****c****d****e****f**